© 2014. Published by The Company of Biologists Ltd | The Journal of Experimental Biology (2014) 217, 2659-2666 doi:10.1242/jeb.104588

RESEARCH ARTICLE

Transition from wing to leg forces during landing in birds

Pauline Provini[1,2,3], Bret W. Tobalske[4], Kristen E. Crandell[4] and Anick Abourachid[1]

ABSTRACT

Transitions to and from the air are critical for aerial locomotion and likely shaped the evolution of flying animals. Research on take-off demonstrates that legs generate greater body accelerations compared with wings, and thereby contribute more to initial flight velocity. Here, we explored coordination between wings and legs in two species with different wingbeat styles, and quantified force production of these modules during the final phase of landing. We used the same birds that we had previously studied during take-off: zebra finch (*Taeniopygia guttata*, *N*=4) and diamond dove (*Geopelia cuneata*, *N*=3). We measured kinematics using high-speed video, aerodynamics using particle image velocimetry, and ground-reaction forces using a perch mounted on a force plate. In contrast with the first three wingbeats of take-off, the final four wingbeats during landing featured ~2 times greater force production. Thus, wings contribute proportionally more to changes in velocity during the last phase of landing compared with the initial phase of take-off. The two species touched down at the same velocity (~1 m s^{-1}), but they exhibited significant differences in the timing of their final wingbeat relative to touchdown. The ratio of average wing force to peak leg force was greater in diamond doves than in zebra finches. Peak ground reaction forces during landing were ~50% of those during take-off, consistent with the birds being motivated to control landing. Likewise, estimations of mechanical energy flux for both species indicate that wings produce 3–10 times more mechanical work within the final wingbeats of flight compared with the kinetic energy of the body absorbed by legs during ground contact.

KEY WORDS: Zebra finch, *Taeniopygia guttata*, Diamond dove, *Geopelia cuneata*, Locomotion, Hindlimb, Forelimb, Particle image velocimetry, PIV

INTRODUCTION

Landing allows the transition from the air to the ground or other substrate. This phase is fundamental to flight, but is often overlooked in studies compared with take-off or cruising flight. Landing places a unique selective pressure upon aerial animals, because a controlled deceleration and descent must be accomplished to avoid injury (Bonser, 1999; Paskins et al., 2007). Animals that do not decelerate properly risk broken wings or legs, or damaged integument: collisions often lead to mortality (Klem, 1990). Thus, understanding this unique aspect of flight performance where legs and wings must coordinate is important in understanding how animal design relates to the ecology, evolution and biomechanics of birds, and even the engineering of autonomous flying vehicles. Herein, we explored the coordination of force production between both legs and wings during landing in birds.

Several lines of evidence indicate that birds carefully control their landing and generally seek to minimize their kinetic energy at touchdown (Warrick et al., 2002) even if some species are eminently capable of targeting in fast flight [for example, a peregrine falcon stooping on a pigeon at relatively fast speed (Alerstam, 1987)]. During landing, birds modulate both wing and tail kinematics to decelerate prior to arriving at the perch (Berg and Biewener, 2010). The distal muscles of the wing, associated with finer-control of the wing surface, show greater motor-unit recruitment during normal landing and birds are unable to coordinate landing when they cannot use these muscles (Dial, 1992a; Dial, 1992b). Landing also requires the integration of the visuomotor system to target and arrive on a landing site safely. This involves the visual system properly processing the changing distance between the bird and perch, and integrating that with the rate of deceleration (Davies and Green, 1990; Lee et al., 1993). Likewise, processing the perch type contributes to changing the landing technique (Green and Cheng, 1998). Given the need for control, we predicted that birds would land at lower velocities than they use to initiate flight even during routine, non-escape take-off (Tobalske et al., 2004; Provini et al., 2012). Consistent with this prediction, prior measurements of ground reaction forces during take-off and landing show that landing forces are ~30% lower (Bonser and Rayner, 1996). This indicates a primary deceleration is accomplished using the wings before touchdown. Here, we used flow visualization techniques to estimate aerodynamic forces during the final phase of landing and, thereby, directly tested the hypothesis about relative wing contribution.

In the light of recent understanding of the unequal contribution of legs and wings during take-off (Provini et al., 2012), we wanted to quantify the contribution of both legs and wings during landing and explore the differences in landing strategies between species with different wing morphology and body size. We used the same zebra finches (*Taeniopygia guttata*, Reichenbach 1862) and diamond doves [*Geopelia cuneata* (Latham 1801)] that we recently studied during take-off (Provini et al., 2012). Zebra finches (12 g, Passeriformes) have rounded, low-aspect ratio wings, while diamond doves (51 g, Columbiformes) have more pointed higher-aspect ratio wings. The two species differ in their wingbeat style and overall flight patterns. We used our previous methods (Provini et al., 2012) to integrate data from wing and body kinematics, ground reaction forces and aerodynamics to improve our understanding of the force transition from the air to the substrate.

RESULTS

Kinematics

Three-dimensional kinematic data of the head and wingtip of birds engaged in descending flight and landing (Fig. 1) showed that body position changed smoothly during the last 12 and the last five wingbeats in zebra finches and diamond doves, respectively. However, the global pattern of the wingbeat trajectory differed from

[1]Muséum National d'Histoire Naturelle, EGB, UMR 7179, 55 Rue Buffon, 75005 Paris, France. [2]Université Paris Descartes, 12 Rue de l'Ecole de Médecine, 75270 Paris, France. [3]Universidade de São Paulo, Instituto de Biociências, Departamento de Zoologia, Rua do Matão, Travessa 14, 101 Butantã 05508090, São Paulo, SP, Brazil. [4]Field Research Station at Fort Missoula, Division of Biological Sciences, University of Montana, Missoula, MT 59812, USA.

*Author for correspondence (pauline.provini@ib.usp.br)

Received 19 March 2014; Accepted 30 April 2014

The Journal of Experimental Biology (2014) doi:10.1242/jeb.104588

List of symbols and abbreviations

A	loop area of wake vortex
$\vec{a}$	acceleration vector
a_h	horizontal component of the acceleration
a_v	vertical component of the acceleration
c	vortex added-mass coefficient
DSUS	downstroke/upstroke transition
D_{wake}	distance between shed vortices
$\vec{F}$	force vector
$\vec{F}_{gr}$	ground reaction force vector
$F_{h,aer}$	horizontal component of the aerodynamic force
$F_{v,aer}$	vertical component of the aerodynamic force
$\boldsymbol{g}$	gravitational acceleration
$\vec{g}$	gravity vector
L	average lift
LE	leg extension
m	body mass
P_i	induced power
PIV	particle image velocimetry
S	width of wake vortex
TD	touch-down
t_{wb}	full wingbeat duration
USDS	upstroke/downstroke transition
V_h	horizontal velocity
V_i	induced velocity
V_v	vertical velocity
V_{wtip}	wingtip velocity
V_{vort}	self-convection velocity of shed vortices
w_{wb}	work per wingbeat
w_{hl}	work absorbed by the hindlimbs
W_0	final full wingbeat
W_{-1}	last but one wingbeat
W_{-2}	second to last wingbeat
W_{-3}	third to last wingbeat
Γ	circulation
ρ	air density
ω	vorticity
ω_{max}	maximum vorticity

that of the third to last wingbeat (W_{-3}) in both species; therefore, we considered landing to begin at the onset of W_{-3}.

In both species, the velocity of the body decreased throughout landing (Fig. 2). In zebra finches, horizontal velocity (V_h) decreased from a mean (±s.d.) of 1.3±0.3 m s^{-1} at the beginning of W_{-3} to 0.82±0.1 m s^{-1} at touch-down (TD), whereas vertical velocity (V_v) started at −0.57±0.1 m s^{-1} and ended at −0.41±0.1 m s^{-1}. Patterns were generally similar in diamond doves, where V_h went from 1.3±0.2 m s^{-1} at the beginning of W_{-3} to 0.81±0.2 m s^{-1} at TD while V_h started at −0.51±0.2 m s^{-1} and ended at −0.27±0.09 m s^{-1}. Then, velocity decreased more rapidly after TD in both species.

The relative timing of leg extension (LE) and final full wingbeat (W_0) differed between species (Fig. 3). During the landing approach, zebra finches started extending their hindlimbs 53±16 ms before TD, which corresponded to the middle of upstroke of the last but one wingbeat (W_{-1}). In diamond doves, LE occurred 137±37 ms before TD, corresponding to the middle downstroke of W_{-3}. In zebra finches, W_0 started 19.8±13.3 ms before TD, which was significantly different from TD (*t*-test: d.f.=14, P<0.0005). In contrast, in doves, W_0 started 8±32 ms after TD, which was not significantly different from TD (*t*-test: d.f.=14, P>0.3).

Differences were apparent between W_0 and the preceding wingbeats although the patterns were not consistent between species. For zebra finches, wingbeats W_{-3} to W_{-1} were 35±0.6 ms in duration, whereas W_0 was only 29±8 ms in duration. In contrast, for diamond doves, mean wingbeat duration for W_{-3} to W_{-1} was 70±5 ms, which was less than the duration of W_0 (79±5 ms).

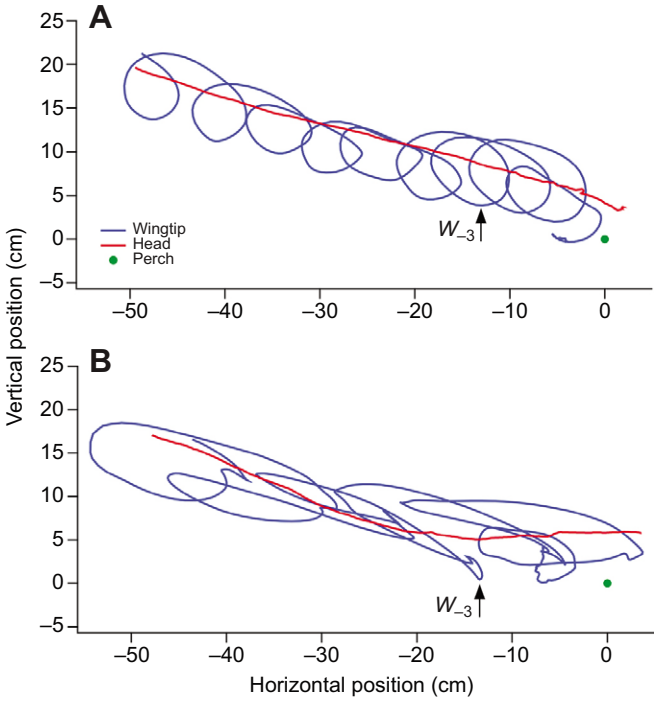

Fig. 1. Horizontal and vertical position of the head (red) and wingtip (blue) of a zebra finch (*Taeniopygia guttata*) and a diamond dove (*Geopelia cuneata*) engaged in descending flight and landing. Twelve wingbeats are shown in zebra finch (A) and six in diamond dove (B). In the present study, we considered landing to begin at the onset of W_{-3}, marked by the vertical arrow on the figure.

Downstroke duration in zebra finches corresponded to 54±1.0% of the whole wingbeat duration for W_{-3} to W_{-1}, whereas downstroke duration decreased to 46.0±0.8% of W_0. For diamond doves, downstroke duration corresponded to 49.1±0.9% of the whole wingbeat duration for W_{-3} to W_{-1} and increased to 58.8±0.8% for W_0 (Fig. 3).

Changes in body angle differed between zebra finches and diamond doves (Fig. 3). In zebra finches, during W_{-3}, body angle was 56±10 deg and was virtually unchanged at TD (58±8 deg) (*t*-test: d.f.=15, P=0.9), with a peak at 65±12 deg after LE. Thereafter, a transition to lower body angles occurred; when the bird reached immobility, its body angle was 24±5 deg. A distinctly different trend was observed for diamond doves: the body angle in W_{-3} started at 49±9 deg, increased to 61±13 deg at TD (statistically different, *t*-test: d.f.=15, P=0.001) and thereafter decreased to 26±7 deg when the diamond doves were motionless.

Force production of the wings

The structure of vortices shed into the wake was complex (Fig. 4), with dispersed vorticity not clearly delineating starting and vortex cores. Moreover, there was intermingling of opposite-sign vorticity in what we interpreted to be the cores, and we consistently observed vorticity near the tail (Fig. 4).

For zebra finches, W_0 produced significantly less lift (L) than the previous wingbeats (ANOVA: factor=wingbeat: $F_{1,22}$=23.41, P<0.0001; factor=individuals: $F_{1,3}$=0.53, P>0.5) (Fig. 5A). Therefore, L during W_0 represented 0.3±0.15 times body weight, whereas it comprised 1.2±0.7 times body weight for W_{-1}, 1.9±0.5 for W_{-2} and 1.9±0.9 for W_{-3}. The aerodynamic force calculated from the particle image velocimetry (PIV) data produced during W_0

The Journal of Experimental Biology (2014) doi:10.1242/jeb.104588

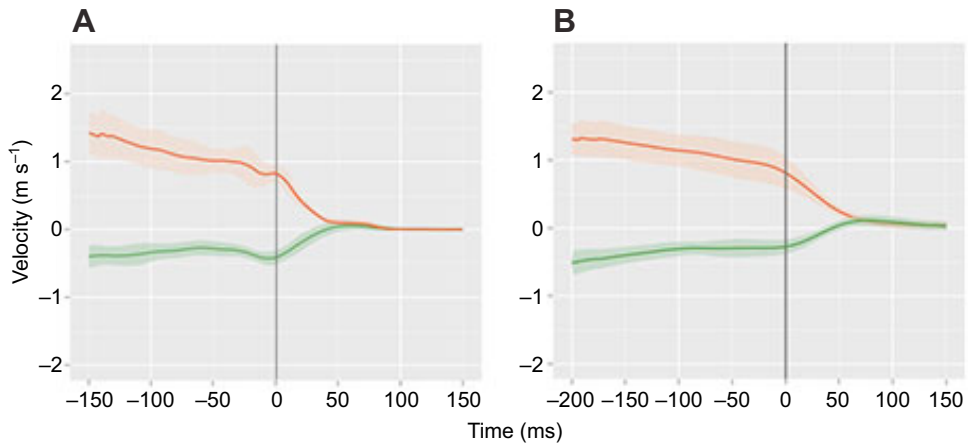

Fig. 2. Velocity calculated from the displacement of the geometric centre of the animal during landing in the zebra finch and diamond dove. *N*=4 zebra finches (A), *N*=3 diamond doves (B), *N*=5 trials within each bird. Envelopes illustrate the variability, defined as the standard deviation across all trials. The horizontal component is shown in orange, the vertical component in green. Time zero is at touch-down (TD), represented by a vertical bar on each graph.

corresponded to 12.9±3.7% of the previous wingbeats (Fig. 5A). There was no significant difference in aerodynamic forces between W_{-3} and W_{-2} (*t*-test: d.f.=9.59, P=0.9); however, there was a significant difference between W_{-2} and W_{-1} (*t*-test: d.f.=13.4, P=0.003) and between W_{-3} and W_{-1} (*t*-test: d.f.=9.9, P=0.03) (Table 1, Fig. 5A).

For diamond doves, W_0 also produced significantly less L than the previous wingbeats (ANOVA: factor=wingbeat: $F_{1,32}$=19.7, P<0.0001; factor=individuals: $F_{1,2}$=1.6, P>0.1). Therefore, L during W_0 represented 0.2±0.2 times body weight, whereas it comprised 0.6±0.5 times body weight for W_{-1}, 1.1±0.6 for W_{-2} and 1.2±0.4 for W_{-3}. The aerodynamic force produced during W_0 corresponded to 15±3% of the previous wingbeats (Fig. 5B). There was no significant difference between the forces calculated from the PIV data between W_{-3} and W_{-2} (*t*-test: d.f.=9.1, P=0.5) whereas there was a significant difference between W_{-2} and W_{-1} (*t*-test: d.f.=10.7, P=0.01) and between W_{-3} and W_{-1} (*t*-test: d.f.=21.6, P<0.001). The whole-body acceleration was fully supported by the wing forces from W_{-3} to W_{-1}. At W_{-1}, this whole-body acceleration was no longer constant; instead it started to decrease and was no longer supported by the wing production of lift.

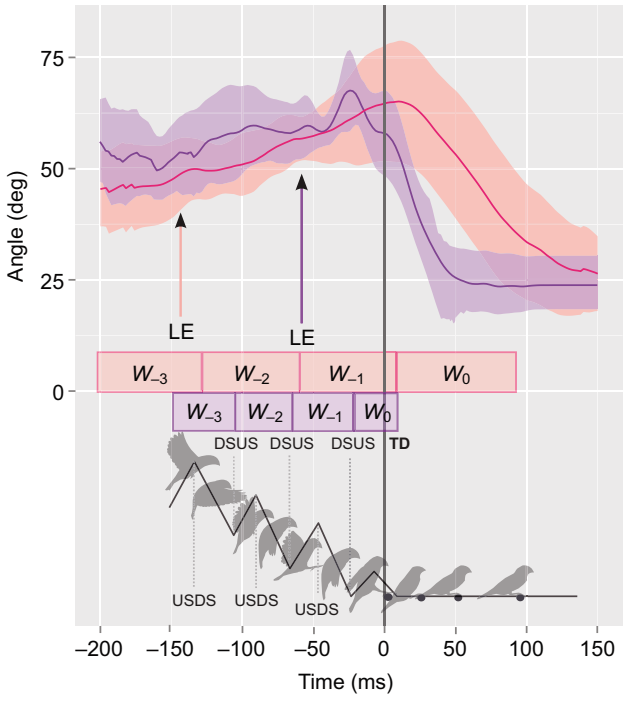

Fig. 3. Body orientation in the zebra finch (purple) and diamond dove (pink) during landing. The succession of wingbeats has been added with boxes corresponding to each wingbeat and the timing of leg extension (LE); time zero is at touch-down (TD). A sketch of the upstroke/downstroke succession during landing in zebra finch is shown below. USDS, upstroke/downstroke transition; DSUS, downstroke/upstroke transition.

Considering the relevant variables for estimating L (Eqn 1, see Materials and methods; Table 1) the differences distinguishing W_0 from the other wingbeats in both species were due to lower circulation (Γ) and smaller area (A) swept by the wings (Table 1). Also, in zebra finches, but not in diamond doves, W_0 was relatively shorter in duration (Table 1).

The angle of induced velocity was ~80 deg through landing and did not vary significantly among wingbeats (Table 1; ANOVA: zebra finches: factor=wingbeat: $F_{3,43}$=0.96, P>0.4; factor=individuals: $F_{1,43}$=4.8, P>0.3; for diamond doves: factor=wingbeat: $F_{3,58}$=0.76, P>0.5; factor=individuals: $F_{1,58}$=1.4, P>0.2). The magnitude of the induced velocity decreased with each wingbeat in zebra finches, from 4.7 m s^{-1} in W_{-3} to 2.3 m s^{-1} in W_0; the induced velocity was greatest during W_{-2} in diamond doves, and decreased with subsequent wingbeats to 3.4 m s^{-1} in W_0.

Our 3D kinematic data allowed the calculation of aerodynamic forces during the approach to calculate the resultant aerodynamic forces (Fig. 5). There were no significant differences between the lift forces calculated from the PIV technique (Fig. 5, yellow) and the resultant aerodynamic forces calculated from the Newton equation using kinematic data (Fig. 5, blue), for W_{-3} (*t*-test: zebra finches: d.f.=21.18, P=0.07; diamond doves: d.f.=15, P=0.05), W_{-2} (*t*-test: zebra finches: d.f.=10.1, P=0.1; diamond doves: d.f.=23, P=0.05) and W_{-1} (*t*-test: zebra finches: d.f.=26.4, P=0.08; diamond doves: d.f.=22, P=0.06). However, there was a difference for W_0 (*t*-test: zebra finches: d.f.=15.6, P=0.04; diamond doves: d.f.=8.1, P<0.01).

Force production of legs

We observed a force peak after TD in both species (Fig. 5), but significant differences occurred between species, in both magnitude and timing. The peak force produced during landing was 0.34±0.1 N on the horizontal component and 0.31±0.1 N on the vertical component in zebra finches and occurred 12±1 ms after TD, compared with 0.56±0.2 N on the horizontal component and 0.72±0.3 N on the vertical component, 22.0±0.9 ms after TD in diamond doves.

There were no significant differences between the forces measured by the force plate (Fig. 5, pink) and the forces deduced from the kinematic data (Fig. 5, blue) (*t*-test: zebra finches: d.f.=29.4, P=0.8; diamond doves: d.f.=79, P=0.06).

The Journal of Experimental Biology (2014) doi:10.1242/jeb.104588

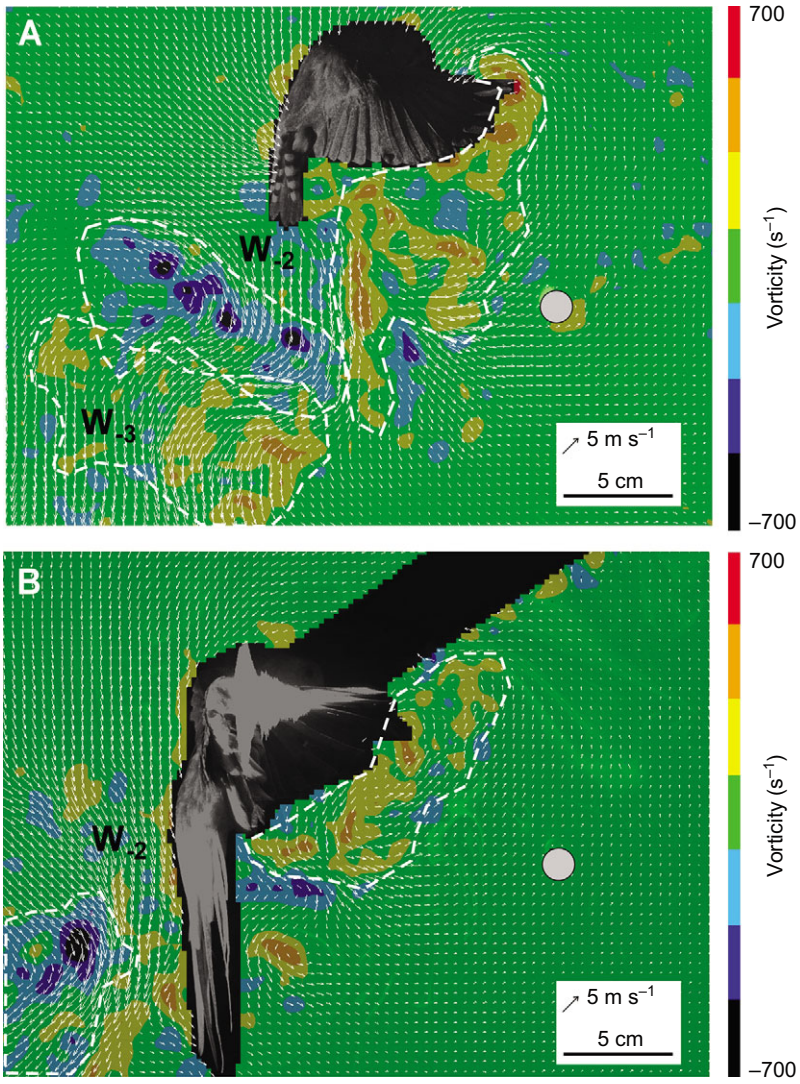

Fig. 4. Particle image velocimetry (PIV) during landing. Velocity vectors ($m s^{-1}$) and, in the background, vorticity (ω, s^{-1}) for the second wingbeat prior to landing (W_{-2}) in (A) zebra finch, with the bird at DSUS, and (B) diamond dove, with the bird at mid-upstroke. The ending vortex for W_{-3} is also visible for the finch in A. Dashed lines indicate regions sampled for ω. Negative-signed ω (blue) indicates the starting vortex; positive signed ω (red) indicates the ending vortex. The grey circle highlights the location of the landing perch.

Comparison of wings and legs contribution during landing

Comparison of the aerodynamic forces with the ground reaction forces revealed that there was a significant difference between the forces generated during W_{-3} to W_0 and the forces generated on the force plate during the peak force (*t*-test: W_{-3} zebra finches: d.f.=31, $P<0.001$; diamond doves: d.f.=35.9, $P=0.001$; W_{-2} zebra finches: *t*-test: d.f.=33.0, $P<0.001$; diamond doves: d.f.=37.7, $P<0.001$; W_{-1} zebra finches: *t*-test: d.f.=31.2, $P<0.001$; diamond doves: d.f.=35.5, $P<0.001$; W_0 zebra finches: *t*-test: d.f.=35.2, $P<0.001$; diamond doves: d.f.=45.3, $P<0.001$) (Fig. 5).

Mechanical work output per wingbeat was ~37 mJ for W_{-3} and W_{-2} in zebra finches and decreased to 16 mJ for W_{-1}. For diamond doves, mechanical work for W_{-3}, W_{-2} and W_{-1}, respectively, was 223, 258 and 128 mJ. Kinetic energy absorbed by the legs was 6 mJ in zebra finches and 26 mJ in diamond doves. The energy absorbed by the legs was therefore 5±2 times less than the per-wingbeat work performed during W_{-3} to W_{-1} in zebra finches and 8±3 times less for the legs compared with the wings in diamond doves.

DISCUSSION

Our results provide new insight into the transition between the air and land in birds by quantifying the transition from wing forces to leg forces through landing in two species of birds with very different landing strategies. In general, the aerodynamic forces produced by the wings were greater during the final phase of landing compared with the initial phase of take-off, and peak ground reaction forces during landing were lower than during take-off (Provini et al., 2012) (Fig. 5). The pattern of lower ground reaction forces during landing than during take-off has also been reported for starlings (Bonser and Rayner, 1996). Therefore, legs did not dominate changes in velocity during the late phase of landing to the same extent that they did during the beginning of take-off. In landing, the hindlimbs reduced velocity by ~60%, whereas in take-off, the hindlimb contribution was ~95% over similar time scales (three wingbeats) (Provini et al., 2012). Coupled with slightly slower velocity at touchdown during landing compared with take-off velocity at the third wingbeat, these results are consistent with the hypothesis that birds are motivated by safety to carefully control landing (Bonser, 1999; Paskins et al., 2007).

Alternative explanations for the greater relative contribution of wings to landing compared with take-off include (1) the prediction that the diminutive mass of the leg musculature would, in the absence of wing activity, not be capable of absorbing the kinetic energy of the body and (2) the possibility that mechanical work contributing to deceleration for the body requires less metabolic energy from the wing muscles compared with the energy required from the leg muscles during the phase of landing featuring ground

The Journal of Experimental Biology (2014) doi:10.1242/jeb.104588

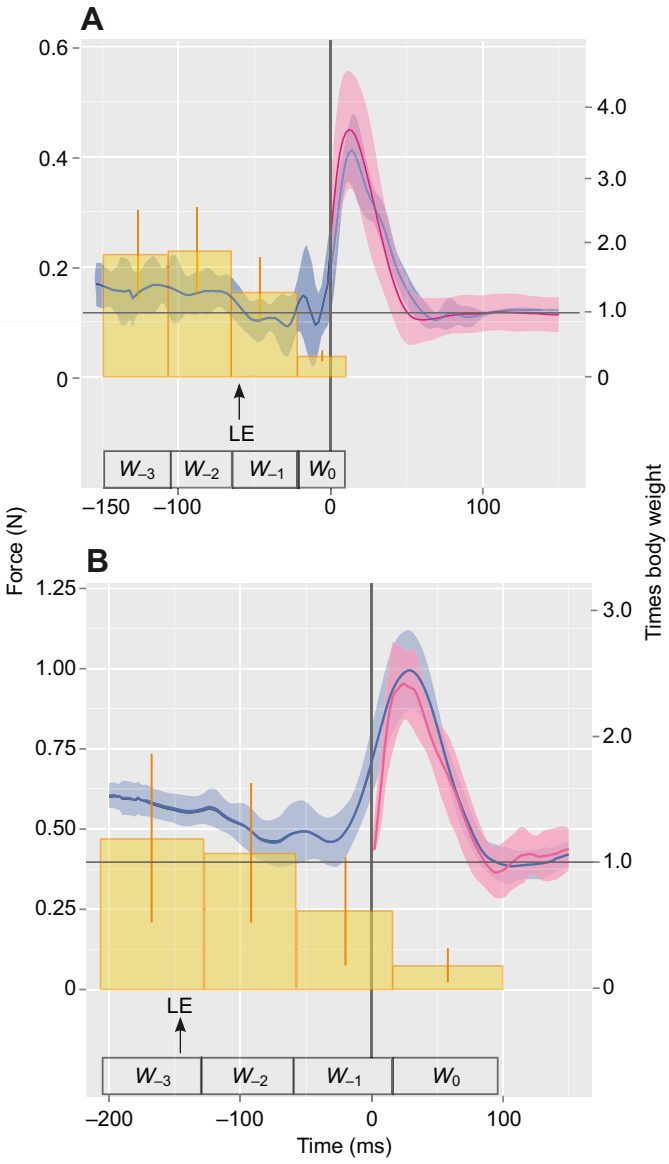

Fig. 5. Forces produced during the last four wingbeats in zebra finches and diamond doves. (A) Zebra finch data, (B) diamond dove data. Blue indicates resultant forces calculated from kinematic data. Pink indicates ground reaction forces calculated using a force plate. Yellow indicates mean aerodynamic forces calculated for each wingbeat using PIV data. For kinematics and force plate measurements, *N*=4 zebra finches, *N*=3 diamond doves, *N*=5 trials within each bird. For PIV data, *N*=30 wingbeats for zebra finches and *N*=38 wingbeats for diamond doves. The succession of wingbeats has been added with boxes corresponding to each wingbeat and the timing of LE; time zero is at TD.

contact. We discount both of these alternatives, but they certainly merit further study. First, the kinetic energy at take-off [about 0.023 J for zebra finches and 0.042 J for diamond doves (Provini et al., 2012)] is greater than the kinetic energy at touchdown (about 0.005 J for zebra finches and 0.018 J for diamond doves), and vertebrate muscle is capable of producing more force during active lengthening than during shortening, and is capable of absorbing more negative than positive work (Hill, 1953; LaStayo et al., 2014). Second, we estimate that the rate of change of kinetic energy within a wingbeat in zebra finches varied from about 0.01 to 0.0017 J from W_{-3} to W_{-1} and was 0.046 J during ground contact from touch-down to the return to support of body weight, while for diamond doves it was 0.0056 to 0.03 J from W_{-3} to W_{-1}, and 0.042 J during ground contact from touchdown to the return to support of body weight. Assuming the metabolic efficiency of vertebrate muscle is 25% and −120% during positive and negative work, respectively (Margaria and Margaria, 1976), the metabolic energy devoted to deceleration per wingbeat varied from 18 to 104% of the energy output during ground contact for zebra finches and between 64 and 342% for diamond doves. Thus, the energy can be dissipated more physiologically economically with some but not all wingbeats prior to touch-down.

As in the present effort, our study of take-off (Provini et al., 2012) involved relaxed, volitional flight generally motivated by the wave of a hand in the vicinity of the bird. Motivational state alters the relative contribution of the hindlimbs to take-off velocity in hummingbirds (Tobalske et al., 2004); thus, we anticipate differences in aerodynamic forces in take-off in zebra finches and diamond doves would be more dramatic if escape or agonistic take-off was included for comparison (Tobalske et al., 2004; Jackson and Dial, 2011).

Interestingly, our data have revealed a stereotyped succession of the forelimb and hindlimb use through landing that differs between species. In zebra finches, TD happens after W_0. This implies a functional separation between the wings and the legs, with the latter entering into locomotion after the wings are inactive. This observation may be related to the concept of modules (Gatesy and Dial, 1996), with a morphological and functional separation of wings and legs in birds. However, in diamond doves, the bird has already reached the perch when W_0 starts. This interesting overlap in the timing of leg extension and wing beating in flight implies that the two modules are not as fully separated in diamond doves as they are in zebra finches. Our two-species comparison is not adequate for testing this idea (Garland and Adolph, 1994), but given the differences in upstroke between zebra finches and diamond doves, future comparative work should seek to explore integration of hindlimb and forelimb modules within phylogenies that include these species (Passeriformes, Columbiformes).

As highlighted above as a major result of our study, wing forces estimated using PIV were greater during landing than during take-off. This was a function of more circulation shed by the wings into the wake rather than aspects of the assumed geometry of the wake, which we made using 3D wing kinematics. Comparing fully airborne wingbeats in landing with those of take-off, circulation was ~1.2 times greater in zebra finches and ~1.3 times greater in diamond doves (Table 1) (Provini et al., 2012). We observed reasonable congruence between aerodynamic forces calculated from the centre of mass kinematics and PIV data for wingbeats other than W_0, where estimated forces from PIV was only 30–40% of acceleration measured using kinematics (Fig. 5). The reason for the discrepancy between the two data sets is linked to the overlap of W_0 with TD and thus to the transition from aerodynamic forces to ground reaction forces (Eqn 3, Materials and methods).

Comparing landing with take-off (Provini et al., 2012), changes in body angle and the angle of induced velocity were consistent with a ‘body reorientation’ hypothesis wherein induced-velocity (downwash) angles during manoeuvres tracks variations as body angle (Berg and Biewener, 2008; Berg and Biewener, 2010; Ros et al., 2011). During the aerial phase of landing, body angle varied from 50 to 65 deg (Fig. 3) and the angle of induced velocity approached perpendicular to horizontal at ~80 deg. During take-off, both angles were smaller: body angle varied from 20 deg relative to the horizontal at lift-off to 35 deg at W_3, and the angle of induced

The Journal of Experimental Biology (2014) doi:10.1242/jeb.104588

Table 1. Aerodynamic parameters for the last four wingbeats in zebra finches (*Taeniopygia guttata*) and diamond doves (*Geopelia cuneata*)

	W_{-3}	W_{-2}	W_{-1}	W_0
Zebra finch (*Taeniopygia guttata*)				
A (cm^2)	151.4±5.7	143.1±6.7	92.4±7.8	31.36±7.3
Γ ($m^2\,s^{-1}$) (+)	0.80±0.3	0.67±0.07	0.46±0.09	0.45±0.05
Γ ($m^2\,s^{-1}$) (–)	−0.62±0.11	−0.50±0.09	−0.51±0.18	−0.29±0.00
S (mm)	60.5±7.9	63.2±11.7	59.9±10.9	56.7±9.3
V_{vort} ($m\,s^{-1}$)	0.79±0.5	0.71±0.2	0.69±0.4	0.71±0.3
Magnitude of induced velocity ($m\,s^{-1}$)	4.7±0.7	4.6±0.9	2.7±0.2	2.3±0.1
Angle of induced velocity to horizontal (deg)	74.2±11	70.1±7	76.8±7	65.9±13
t_{wb} (ms)	35.5±4.1	35.1±3.7	35.8±3.5	28.9±8.3
V_{wtip} ($m\,s^{-1}$)	8.1±1.4	9.4±0.7	6.9±1.0	1.9±0.5
D_{wake} (m)	–	0.18±0.3	0.15±0.1	0.13±0.2
Diamond dove (*Geopelia cuneata*)				
A (cm^2)	499.4±17.0	472.1±2.9	451.3±4.5	295.6±6.7
Γ ($m^2\,s^{-1}$) (+)	0.87±0.1	1.05±0.3	0.63±0.1	0.27±0.2
Γ ($m^2\,s^{-1}$) (–)	−0.91±0.2	−0.93±0.2	−0.59±0.1	−0.24±0.0
S (mm)	67.6±17.6	68.7±15.1	56.8±10.8	60.2±8.1
V_{vort} ($m\,s^{-1}$)	0.85±0.3	0.83±0.2	0.75±0.4	0.74±0.5
Magnitude of induced velocity ($m\,s^{-1}$)	3.9±0.4	4.9±0.1	3.7±0.5	3.4±0.3
Angle of induced velocity to horizontal (deg)	81.0±11	77.4±4	76.3±2	69.9±3
t_{wb} (ms)	65.2±3.4	66.7±4.5	73.7±3.7	78.8±7.0
V_{wtip} ($m\,s^{-1}$)	11.8±0.2	11.3±1.4	8.4±4.2	4.2±2.7
D_{wake} (m)	–	0.26±0.3	0.25±0.4	0.20±0.3

W_{-3} to W_0 represent the last four wingbeats before landing. Data are means ± s.d.
A, loop area of vortex wake; Γ, circulation (positive or negative); S, width of wake vortex; V_{vort}, self-convection velocity of shed vortices; t_{wb}, full wingbeat duration; V_{wtip}, wingtip velocity; D_{wake}, distance between shed vortices.

velocity was 60–70 deg in both species during take-off (Provini et al., 2012).

Current understanding of the relative contributions of the forelimb and hindlimb modules to velocity during take-off and landing needs to be placed in the broader context of avian flight. The existing studies of take-off interpret that the legs dominate, and have also focused on at most three wingbeats (Earls, 2000; Tobalske et al., 2004; Provini et al., 2012). Once in the air, changes in velocity are the exclusive domain of the wings, rather than the legs. Exceptions may include birds modulating drag using their legs in some circumstances; for example, for stability in turbulence (Combes and Dudley, 2009). Birds of similar size and phylogeny as the species in our study routinely fly at around 15 $m\,s^{-1}$ during migratory flights (Bruderer and Boldt, 2001). Flight speeds between foraging substrates in small woodpeckers (Piciformes, birds that routinely use flap-bounding like the finches) is ~10 $m\,s^{-1}$ (Tobalske, 1996). Therefore, the potentially overlooked – yet obvious – conclusion is that, overall, the forelimbs dominate the modulation of velocity in flying birds, and the relative contribution of the legs to transitions between substrates is partly a function of the arbitrary time scale researchers use to delineate the end of take-off or the beginning of landing (Fig. 1). Underscoring this, and helping to account for the significant mass difference between the wing muscles and those of the legs of flying birds, our estimates of mechanical work per wingbeat during W_{-3} to W_{-1} of landing were 3–10 times greater than energy absorption by the legs during ground contact.

This study integrates for the first time aerodynamics with kinematics and ground reaction force measurements during the final phase of landing, and revealed that birds appear to control their landing by producing larger wing forces in the final wingbeats prior to touchdown compared with the initial wingbeats during take-off. The hindlimbs nevertheless function significantly in changing velocity during the final phase of landing and are, therefore, critical to the absorption of kinetic energy after touchdown. To improve understanding of how birds modulate velocity when moving in the three vastly different substrates on earth (air, land and water), it will remain important to frame transitions between substrates in the context of sustained locomotion within substrates. In this way, our results will inform future efforts to understand the ecology and evolution of transitions to and from the air.

MATERIALS AND METHODS

Animals

Four zebra finches (*T. guttata*; mean ± s.d. body mass 12.3±0.21 g) and three diamond doves (*G. cuneata*; 51.0±5.1 g) were purchased from commercial dealers, housed in flight cages, and provided with food and water *ad libitum*.

The data were obtained with the same experimental protocol as described previously (Provini et al., 2012) other than the direction of bird flight, so we abbreviate our description of our methods here. Kinematics, force and PIV data collection were performed at the Field Research Station in Missoula, MT, USA. The animals were trained to land on a perch at a descent angle of about 45 deg, with a 1 m flight path distance between their take-off and landing perches. All care and experimental procedures were approved by the University of Montana IACUC.

Kinematics

We used four digital high-speed video cameras, including two Photron 1024 PCI, one Photron SA-3 (Photron, Inc., San Diego, CA, USA) and one Phantom MiroEx4 (Vision Research Inc., Wayne, NJ, USA) sampling at 500 Hz with a shutter speed of 200 µs. We focused our analysis upon the final four wingbeats of landing that ended with the bird motionless on the perch. Three-dimensional motion of the wings was used to estimate average aerodynamic force per wingbeat (see below). Measures of whole-body velocity and acceleration were computed using 2D, lateral-view videos obtained from one Photron 1024 PCI camera.

We used a conventional frame of reference (vertical axis pointing upward, horizontal axis in the direction of the forward movement of the animal). The vertical trajectory of tip of the ninth primary was used to define flight phases as it describes a succession of local maxima and minima that match the upstroke/downstroke transition (USDS) and downstroke/upstroke transition (DSUS), respectively.

We classified the wingbeats of landing as described elsewhere (Berg and Biewener, 2010). The last wingbeat amplitude was usually lower than that during the preceding wingbeats and this final wingbeat (W_0) led directly to the final repositioning of the wings during perching. The previous three wingbeats were numbered backwards. We measured the onset of leg extension (LE) during flight. Touch-down (TD) was defined as the first contact of the perch by the feet.

Ground reaction forces

The force perch was the same as that used previously (Provini et al., 2012), mounted to a custom-designed Bertec force plate (15×15 cm platform, 200 Hz resonant frequency; Bertec Corp., Columbus, OH, USA). Forces on the Bertec plate were digitally amplified 10 times (Bertec AM6800) and recorded at 500 Hz using Chart software v4.5 (ADInstruments Inc., Colorado Springs, CO, USA) and a Powerlab 8 SP A/D converter (ADInstruments Inc.).

Forces were filtered using a zero phase shift low-pass (50 Hz) Butterworth filter. Because landing implied forces in both directions as well as acceleration and deceleration, it was clearer to work with forces, instead of accelerations. Therefore, unlike in our previous study (Provini et al., 2012), we did not subtract body weight [=body mass (m) × gravitational acceleration ($\boldsymbol{g}$)] from the force recordings but we used the equation of Newton and included body weight in the equation (see below).

PIV

To compare aerodynamics with associated wingbeat kinematics, we used a synchronized high-speed video camera (Photron 1024 PCI) sampling at 500 Hz, located lateral to the animal. Data acquisition and analysis of PIV were performed using a LaVison GmBH (Goettingen, Germany) PIV system running DaVis 7.1 software. See our previous study (Provini et al., 2012) for additional details.

We estimated average lift during the entire wingbeat (L) by coupling our PIV data with the three-dimensional kinematic data for the same test subjects (Spedding et al., 2003; Warrick et al., 2005; Tobalske and Dial, 2007) (see 'Kinematics', above). Note that L includes vertical (weight support) and horizontal (thrust) components. Average L was estimated as:

$$L = \rho \frac{A(\Gamma + cSV_{\text{vort}})}{t_{\text{wb}}}, \quad (1)$$

where ρ is air density (air density in Missoula at 1000 m altitude is 1.06±0.01 kg m^{-3}), A is the area swept by the two wings during each downstroke, not including the body, c is the added-mass coefficient (Dabiri, 2005), S is the average diameter of the observed vortex cores and V_{vort} is the self-induced vortex velocity (Dabiri, 2005). Following previous studies (Spedding et al., 2003; Warrick et al., 2005), we assumed that a single vortex loop was shed per downstroke and that no contraction occurred during wake development. We assumed c=0.72 as the added-mass coefficient previously reported for an elliptical vortex (Dabiri, 2005). We measured V_{vort} as the observed rate of translation of maximum vorticity (ω_{max}) in the subset (N=37 for zebra finches and N=42 for diamond doves) of our PIV samples in which the same vortex core appeared in consecutive images. We also measured the magnitude and angle from horizontal for induced velocity (m s^{-1}) in the middle of the shed vortices (Tobalske and Dial, 2007) as well as the angle of induced velocity compared with the horizontal (in deg).

Comparison between data sets

In order to compare the three data sets (wing and body kinematics, ground reaction forces, and aerodynamics) we used the equation of motion:

$$\sum \vec{F} = m\vec{a}, \quad (2)$$

where $\vec{F}$ (in N) corresponds to the forces applied on the bird, m (in kg) corresponds to the mass of the bird and $\vec{a}$ (in m s^{-2}) is the acceleration of the animal.

In this specific case:

$$\overrightarrow{F_{\text{aer}}} + \overrightarrow{F_{\text{gr}}} + m\vec{g} = m\vec{a}, \quad (3)$$

where $\overrightarrow{F_{\text{aer}}}$ corresponds to the aerodynamic forces produced by the bird when in the air (calculated from the PIV data), $\overrightarrow{F_{\text{gr}}}$ corresponds to the ground reaction forces on the perch (calculated from the force plate) and $\vec{g}$ corresponds to the gravity (magnitude of the vector is −9.81 m s^{-2}). During the approach phase of landing, before the bird touches the perch, $\overrightarrow{F_{\text{gr}}}$ is zero.

On the vertical axis:

$$F_{\text{v,aer}} + F_{\text{v,gr}} + m\boldsymbol{g} = ma_{\text{v}}. \quad (4a)$$

On the horizontal axis:

$$F_{\text{h,aer}} + F_{\text{h,gr}} = ma_{\text{h}}. \quad (4b)$$

The v exponent corresponds to the vertical component of the force or acceleration and the h subscript to the horizontal component.

We averaged kinematic and PIV data among birds within each species to obtain a rough estimate of mechanical energy flux within wingbeats and during ground contact. For simplicity, we assumed all mechanical power output by the wings was measurable as net force acting on the body (Eqn 1) multiplied by induced velocity (V_{i}). Using a Rankine–Froude momentum jet model (e.g. Pennycuick, 1975) and treating the wings as an actuator disc:

$$V_{\text{i}} = \frac{m\boldsymbol{g}}{2V\rho A}. \quad (5)$$

The standard application of the momentum jet model assumes V_{i} in the contracted wake is double that at the actuator disc; however, we used our empirical measures of V_{i} in the centre of shed vortices as these values were 7±9% of those predicted by the simple model for wingbeats W_{-3} and W_{-2}. To estimate induced power (P_{i}), the dominant form of aerodynamic power in slow flight (Pennycuick, 1975), we used:

$$\vec{P}_{\text{i}} = V_{\text{i}}(\overrightarrow{F_{\text{aer}}} + \overrightarrow{F_{\text{gr}}}). \quad (6)$$

Work per wingbeat was thus:

$$w_{\text{wb}} = P_{\text{i}} t_{\text{wb}}. \quad (7)$$

We assumed the energy absorbed by the hindlimbs during landing (w_{hl}) was the total kinetic energy of the bird at touchdown:

$$w_{\text{hl}} = \frac{1}{2} mV^2. \quad (8)$$

Because of the many simplifying assumptions intrinsic to our estimates of aerodynamic work, and the mixed contribution of W_0 and the legs to energy flux during the initial phase of ground contact, the values we report should be interpreted with caution and used only as a general index.

Statistics

To test for differences in the timing of last downstroke and TD, we used two-way repeated measures ANOVA with time and individual as factors and taking into account the trial repetition and species. We also used two-way repeated measures ANOVA to test for a statistically significant difference between wingbeats (W_{-3} to W_0) for L, the angle magnitude of induced velocity in the wake. Wingbeat and individual were used as factors and the trial repetition was also taken into account for both species. Lastly, t-tests were used to compare data sets coming from kinematic analysis with data sets coming from ground reaction force or aerodynamic analyses. All statistical tests were performed using R package *stats* version 2.15.0 (R Development Core Team, 2010). Throughout, we report means ± s.d.

Acknowledgements

We are grateful to Brandon Jackson for his help during the experiments. Thanks to the two anonymous reviewers for their insights and their help in clarification of the manuscript.

Competing interests

The authors declare no competing financial interests.

Author contributions

P.P. and B.W.T. were involved in the conception, design and execution of the study, and interpretation of the findings, and drafted and revised the article. K.E.C was involved in the design and execution of the study, interpretation of the findings, and drafting and revising the article. A.A. was involved in the conception of the study and revising the article.

Funding
This research was supported by grants from the UMR 7179, l'Action Transversale du Muséum National d'Histoire Naturelle formes possibles, formes réalisées and from Ecole Doctorale Frontières du Vivant and Bettencourt-Schueller foundation fellowships as well as the National Science Foundation [grant nos IOS-0923606 and IOS-0919799].

References

Alerstam, T. (1987). Radar observations of the stoop of the peregrine falcon *Falco peregrinus* and the goshawk *Accipiter gentilis*. *Ibis* **129**, 267-273.
Berg, A. M. and Biewener, A. A. (2008). Kinematics and power requirements of ascending and descending flight in the pigeon (*Columba livia*). *J. Exp. Biol.* **211**, 1120-1130.
Berg, A. M. and Biewener, A. A. (2010). Wing and body kinematics of takeoff and landing flight in the pigeon (*Columba livia*). *J. Exp. Biol.* **213**, 1651-1658.
Bonser, R. H. C. (1999). Branching out in locomotion: the mechanics of perch use in birds and primates. *J. Exp. Biol.* **202**, 1459-1463.
Bonser, R. and Rayner, J. (1996). Measuring leg thrust forces in the common starling. *J. Exp. Biol.* **199**, 435-439.
Bruderer, B. and Boldt, A. (2001). Flight characteristics of birds. *Ibis* **143**, 178-204.
Combes, S. A. and Dudley, R. (2009). Turbulence-driven instabilities limit insect flight performance. *Proc. Natl. Acad. Sci. USA* **106**, 9105-9108.
Dabiri, J. O. (2005). On the estimation of swimming and flying forces from wake measurements. *J. Exp. Biol.* **208**, 3519-3532.
Davies, M. N. O. and Green, P. R. (1990). Optic flow-field variables trigger landing in hawk but not in pigeons. *Naturwissenschaften* **77**, 142-144.
Dial, K. P. (1992a). Activity patterns of the wing muscles of the pigeon (*Columbia livia*) during different modes of flight. *J. Exp. Zool.* **262**, 357-373.
Dial, K. P. (1992b). Avian forelimb musches and nonsteady flight – can birds fly without using the muscles in their wings? *Auk* **109**, 874-885.
Earls, K. D. (2000). Kinematics and mechanics of ground take-off in the starling Sturnis vulgaris and the quail *Coturnix coturnix*. *J. Exp. Biol.* **203**, 725-739.
Garland, T. and Adolph, S. C. (1994). Why not to do two-species comparative studies: limitations on inferring adaptation. *Physiol. Zool.* **67**, 797-828.
Gatesy, S. M. and Dial, K. P. (1996). Locomotor modules and the evolution of avian flight. *Evolution* **50**, 331-340.
Green, P. R. and Cheng, P. (1998). Variation in kinematics and dynamics of the landing flights of pigeons on a novel perch. *J. Exp. Biol.* **201**, 3309-3316.
Hill, A. V. (1953). The mechanics of active muscle. *Proc. R. Soc. B* **141**, 104-117.
Jackson, B. E. and Dial, K. P. (2011). Scaling of mechanical power output during burst escape flight in the Corvidae. *J. Exp. Biol.* **214**, 452-461.
Klem, D., Jr (1990). Collisions between birds and windows: mortality and prevention (Colisiones de pájaros con ventanas: mortalidad y prevención). *J. Field Ornithol.* **61**, 120-128.
LaStayo, P., Marcus, R. L., Dibble, L., Frajacomo, F. and Lindstedt, S. L. (2014). Eccentric exercise in rehabilitation: safety, feasibility and application. *J. Appl. Physiol.* **116**, 1426-1434.
Lee, D. N., Davies, M. N. O., Green, P. R. and Van Der Weel, F. R. R. (1993). Visual control of velocity of approach by pigeons when landing. *J. Exp. Biol.* **180**, 85-104.
Margaria, R. and Margaria, R. (1976). *Biomechanics and Energetics of Muscular Exercise*. Oxford: Clarendon Press.
Paskins, K. E., Bowyer, A., Megill, W. M. and Scheibe, J. S. (2007). Take-off and landing forces and the evolution of controlled gliding in northern flying squirrels *Glaucomys sabrinus*. *J. Exp. Biol.* **210**, 1413-1423.
Pennycuick, C. J. (1975). Mechanics of flight. In *Avian Biology*, Vol. 5 (ed. D. S. Farner and J. R. King), pp. 1-75. New York, NY: Academic Press.
Provini, P., Tobalske, B. W., Crandell, K. E. and Abourachid, A. (2012). Transition from leg to wing forces during take-off in birds. *J. Exp. Biol.* **215**, 4115-4124.
R Development Core Team (2010). *R: A Language and Environment for Statistical Computing*. R Foundation for Statistical Computing, Vienna, Austria. Available at: http://www.R-project.org/.
Ros, I. G., Bassman, L. C., Badger, M. A., Pierson, A. N. and Biewener, A. A. (2011). Pigeons steer like helicopters and generate down- and upstroke lift during low speed turns. *Proc. Natl. Acad. Sci. USA* **108**, 19990-19995.
Spedding, G. R., Rosén, M. and Hedenström, A. (2003). A family of vortex wakes generated by a thrush nightingale in free flight in a wind tunnel over its entire natural range of flight speeds. *J. Exp. Biol.* **206**, 2313-2344.
Tobalske, B. W. (1996). Scaling of muscle composition, wing morphology, and intermittent flight behavior in woodpeckers. *Auk* **113**, 151-177.
Tobalske, B. W. and Dial, K. P. (2007). Aerodynamics of wing-assisted incline running in birds. *J. Exp. Biol.* **210**, 1742-1751.
Tobalske, B. W., Altshuler, D. L. and Powers, D. R. (2004). Take-off mechanics in hummingbirds (Trochilidae). *J. Exp. Biol.* **207**, 1345-1352.
Warrick, D. R., Bundle, M. W. and Dial, K. P. (2002). Bird maneuvering flight: blurred bodies, clear heads. *Integr. Comp. Biol.* **42**, 141-148.
Warrick, D. R., Tobalske, B. W. and Powers, D. R. (2005). Aerodynamics of the hovering hummingbird. *Nature* **435**, 1094-1097.